A NO-REFERENCE FIDELITY METRIC ENABLING HYPERSPECTRAL SUPER RESOLUTION BEYOND DATASET RESOLUTION LIMITS

Nour Aburaed[1*], *Marouane Tliba*[2,3*], *Aladine Chetouani*[3], *Faouzi Alaya Cheikh*[4], *Rachid Jennane*[2], *Azeddine Beghdadi*[3]

[1]College of Engineering and IT, University of Dubai, Dubai, UAE
[2]University of Orleans, IDP UMR CNRS Laboratory, Orleans, France
[3]Universite Sorbonne Paris Nord, L2TI, Paris, France
[4]Norwegian University of Science and Technology (NTNU), Gjovik, Norway

ABSTRACT

Hyperspectral Image (HSI) Super Resolution (SR) is traditionally developed and evaluated under a synthetic training paradigm, where high-resolution cubes are artificially downsampled and networks are optimized to reconstruct the original spatial resolution. While effective for controlled benchmarking, this approach has an intrinsic limitation: SR performance can only be assessed at the native sensor resolution of the available datasets, making quantitative evaluation impossible when SR must extrapolate to higher spatial scales that cannot be physically acquired in biomedical systems. Conventional fidelity metrics, such as Spectral Angle Mapper (SAM) and ERGAS, therefore fail in practical deployment scenarios, where no high-resolution reference exists. In this paper, we introduce a no-reference objective fidelity metric for hyperspectral super-resolution, learned from paired LR–HR cubes across two biomedical datasets (HyperSkin and In-Vivo Brain). The proposed model predicts expected spatial–spectral fidelity scores directly from reconstructed HSI patches to enable accurate quality estimation (PLCC above 0.99) without access to the ground-truth high-resolution cube. The proposed approach bridges the gap between synthetic SR training protocols and real-world deployment by offering a scalable and practically meaningful solution for assessing hyperspectral super-resolution quality.

***Index Terms*—** Hyperspectral Imaging, Super-Resolution, No-Reference Quality Assessment, Spectral Angle Mapper, ERGAS, Blind Distortion Estimation

1. INTRODUCTION

Super Resolution (SR) for Hyperspectral Imaging (HSI) has progressed rapidly, driven by advances in 3D convolutional networks, spectral–spatial transformers [1, 2, 3], and frequency-domain architectures [4]. Yet almost all existing HSI-SR studies share one evaluation protocol: a high-resolution cube is treated as ground-truth, synthetically degraded, super-resolved, and assessed using reference-based metrics such as the Spectral Angle Mapper (SAM) and ERGAS. From a signal processing perspective, SAM measures the angular deviation between two high-dimensional spectral signals, while ERGAS quantifies relative spatial–spectral reconstruction error [5]. In real deployment, however, true high-resolution signals are rarely available, especially in biomedical HSI, where physical constraints and acquisition time prevent capturing detailed spectral signatures, leaving SAM and ERGAS incomputable without a reference.

This reveals a critical gap. Prior No-Reference Image Quality Assessment (NR-IQA) for hyperspectral restoration and fusion [6, 7, 8], and more recent blind quality prediction via learned feature ranking [9], are not designed for SR distortion and do not estimate SAM, ERGAS, or related spectral-specific measures. No-reference assessment of RGB SR outputs using deep and frequency-domain models [10] reflects growing interest in reference-free evaluation, but does not extend to spectral distortion in super-resolved hyperspectral data.

To address this, we learn proxy spectral fidelity metrics that apply directly to super-resolved outputs when no reference exists. Our approach differs from prior no-reference HSI quality assessment in three ways, as summarized in the contributions below.

We evaluate existing HSI-SR models in two complementary regimes: the classical full-reference protocol (downsampling $\rightarrow$ SR $\rightarrow$ SAM/ERGAS), and real SR beyond the dataset's intrinsic resolution, assessed solely through our learned proxy metrics. **The contributions of this work are threefold:**

1. We propose a learning based framework for reference-free spectral evaluation,predicting proxy SAM and ERGAS estimates directly from super-resolved hyperspectral data and overcoming the inability to assess real SR beyond dataset resolution.

2. We construct an augmented distortion corpus derived

* Equal contribution; the author order is equivalent.

from heterogeneous SR models and training stages, capturing the intrinsic spectral-spatial error behavior of modern SR networks.

3. We introduce a benchmarking paradigm that integrates classical full-reference evaluation with real, reference-free SR assessment, yielding reliable, spectrally meaningful quality estimates in both regimes.

2. PROBLEM FORMULATION

Hyperspectral signals exhibit strong spectral redundancy and low-rank structure, where most spectral variability lies in a small subspace spanned by a few dominant signatures [11]. SR distortions therefore manifest as systematic angular deviations in this subspace rather than arbitrary noise. Neighboring bands are highly correlated due to spectral smoothness, making spectral shape distortions spatially and spectrally consistent across the cube [12]. As a result, both the distribution of spectral angles and the spatial–spectral reconstruction error follow predictable patterns inferable from the reconstructed signal alone, so global indicators such as mean SAM and ERGAS can be approximated from intrinsic spectral–spatial statistics without a ground-truth reference.

Let $X \in \mathbf{R}^{H\times W\times B}$ denote a super-resolved hyperspectral cube, where H, W, and B are the spatial height, width, and number of spectral bands. For each location (i, j), the spectral vector is $\mathbf{x}_{ij} \in \mathbf{R}^B$. In conventional HSI-SR evaluation, spectral fidelity is quantified using the SAM, defined between a reconstructed vector $\mathbf{x}_{ij}$ and its ground-truth counterpart $\mathbf{y}_{ij}$ as:

$$\mathrm{SAM}(\mathbf{x}_{ij}, \mathbf{y}_{ij}) = \arccos\left(\frac{\mathbf{x}_{ij}^\top \mathbf{y}_{ij}}{\|\mathbf{x}_{ij}\|\|\mathbf{y}_{ij}\|}\right). \tag{1}$$

In conventional evaluation, angular distortion is summarized by the mean SAM, which requires y_{ij} and therefore cannot be computed when no reference is available:

$$\mu_{\mathrm{SAM}} = \frac{1}{HW}\sum_{i=1}^{H}\sum_{j=1}^{W}\mathrm{SAM}(\mathbf{x}_{ij}, \mathbf{y}_{ij}). \tag{2}$$

On the other hand, ERGAS provides a complementary measure of spatial–spectral reconstruction error as seen in the following equation:

$$ERGAS = 100 \cdot \frac{1}{r}\sqrt{\frac{1}{B}\sum_{b=1}^{B}\left(\frac{\mathrm{RMSE}_b}{\mu_b}\right)^2}, \tag{3}$$

where r is the spatial resolution ratio, $RMSE_b$ is the Root Mean Squared Error for band b, μ_b is the mean intensity of the corresponding reference band.

From a signal processing perspective, μ_{SAM} reflects the angular deviation of the reconstructed spectral subspace, whereas ERGAS captures relative deviation in spatial and spectral energy. Equations (2) and (3) define the conventional full-reference computation of mean SAM and ERGAS and are used only to generate supervision during training. In practical deployment, the ground-truth spectra y_{ij} and the mean reference intensity μ_b are unavailable, and these quantities cannot be computed directly.

To enable evaluation in the absence of ground-truth data, we formulate the estimation of mean SAM and ERGAS as a blind regression problem. Specifically, a function $f_\theta(\cdot)$ is learned to predict the global distortion indicators directly from the reconstructed hyperspectral cube X, without access to reference spectra. This is expressed in the following equation:

$$\hat{\mu}_{\mathrm{SAM}} = f_\theta^{(1)}(X), \qquad \widehat{\mathrm{ERGAS}} = f_\theta^{(2)}(X), \tag{4}$$

where $f_\theta^{(1)}(\cdot)$ and $f_\theta^{(2)}(\cdot)$ map the reconstructed signal to estimates of mean SAM and ERGAS. During inference, the proposed estimators operate solely on the reconstructed signal X, and no reference information is required.

3. LEARNING-BASED QUALITY PREDICTION NETWORKS

This section presents the core contribution of this work: a learning-based framework for predicting reference-based hyperspectral fidelity metrics directly from super-resolved data. Unlike prior no-reference HSI quality assessment methods that rely on generic perceptual features or ranking-based scores, the proposed approach learns proxy estimators for SAM and ERGAS, which are tightly coupled to hyperspectral super-resolution fidelity. The architectures introduced in this section differ only in how spatial, spectral, and spectral-frequency information is encoded to model these distortions.

To enable reference-free spectral fidelity prediction, we develop a family of hyperspectral quality–regression networks, culminating in a Frequency-Enhanced Global Attention model (FEGAN), which constitutes the main proposed architecture of this work. Given an input cube $\mathbf{X}\in\mathbb{R}^{H\times W\times S}$, each model realizes $\hat{q} = f_{\boldsymbol{\theta}}(\mathbf{X})$, where $\hat{q}$ estimates a reference distortion measure (SAM or ERGAS). The three architectures differ in how they encode spatial structure, spectral correlation, and frequency-domain information. Bold symbols (e.g., $\mathbf{X}, \mathbf{W}$) denote tensors or learnable network parameters, while non-bold symbols (e.g., H, W) represent spatial dimensions as defined in Section 2.

3.1. Spatial Feature Regression Network (SFRN)

As a baseline variant, SFRN treats the spectral dimension as stacked channels and learns spatial descriptors via two convolutions:

$$\mathbf{F}^{(1)} = \sigma(\mathbf{W}^{(1)} * \mathbf{X}), \qquad \mathbf{F}^{(2)} = \sigma(\mathbf{W}^{(2)} * \mathbf{F}^{(1)}) \tag{5}$$

where $\sigma(\cdot)$ denotes a pointwise non-linear activation function (ReLU in all experiments). This is followed by a downsampling operator $D(\cdot)$ producing $\mathbf{U} = D(\mathbf{F}^{(2)})$. A global average pooling step yields $\bar{\mathbf{u}} = \frac{1}{HW}\sum_{h,w}\mathbf{U}_{:,h,w}$, which is mapped to $\hat{q}$ through a lightweight Multilayer Perceptron (MLP) consisting of two fully connected layers with a small hidden dimension. As spectral bands do not interact explicitly, SFRN models *spatial* distortion patterns such

as local blurring, ringing artifacts, and spatial inconsistency introduced by super-resolution.

3.2. Frequency-Modulated Spectral-Spatial Attention Network (FSSAN)

As an intermediate variant, FSSAN extends SFRN by incorporating spectral-frequency modulation through attention mechanisms. A spectral Discrete Cosine Transform (DCT) transforms the encoded tensor, $\mathbf{Z} = \mathrm{DCT}_S(\mathbf{F})$, and a channel-wise attention weight

$$\mathbf{A}_{\text{spec}} = \sigma\big(\Phi_2(\rho(\Phi_1(\mathbf{Z})))\big), \tag{6}$$

produces modulated coefficients $\mathbf{Z}' = \mathbf{A}_{\text{spec}} \odot \mathbf{Z}$. $\sigma(\cdot)$ denotes a sigmoid activation function, $\phi_1(\cdot)$ and $\phi_2(\cdot)$ are learnable linear transformations implemented as 1×1 convolutions, and $\rho(\cdot)$ represents a non-linear activation (ReLU). The modulated representation Z' is obtained by element-wise multiplication of the spectral attention weights with the DCT coefficients, i.e., $Z' = A_{\text{spec}} \odot Z$.

Applying IDCT_S returns $\mathbf{F}'$, followed by a light spatial-attention refinement and global pooling. By operating jointly in the spectral-frequency and spatial domains, FSSAN captures distortions such as spectral smoothing, band-wise inconsistency, and frequency-domain artifacts that may preserve spatial structure but alter spectral coherence, and are therefore difficult to detect using spatial features alone [13].

3.3. Frequency-Enhanced Global Attention Network (FEGAN)

The operators DCT/IDCT, the activation function σ, and the MHSA module are used here with the same interpretation as described in Subsection 3.2. FEGAN combines spectral–frequency modulation with global spatial attention. Given encoder features $\mathbf{F}$, a spectral DCT produces

$$\mathbf{Z} = \mathrm{DCT}_S(\mathbf{F}) \tag{7}$$

A lightweight excitation module computes spectral weights $\mathbf{A}_c = \sigma\big(\Phi(\mathrm{AvgPool}(\mathbf{Z})) + \Phi(\mathrm{MaxPool}(\mathbf{Z}))\big)$, which modulate the frequency responses as $\mathbf{Z}' = \mathbf{A}_c \odot \mathbf{Z}$. The tensor is reshaped into spatial tokens $\mathbf{T} \in \mathbb{R}^{B \times HW \times C}$ and refined via two Multi-Head Self-Attention (MHSA) layers,

$$\mathbf{T}^{(k+1)} = \mathrm{MHSA}(\mathbf{T}^{(k)}), \quad k = 0, 1 \tag{8}$$

After folding and inverse DCT, $\mathbf{F}' = \mathrm{IDCT}_S(\mathrm{fold}(\mathbf{T}^{(2)}))$, global pooling and a final MLP yield the estimate $\hat{q}$. This design jointly models spectral–frequency patterns and long-range spatial dependencies within a compact architecture.

4. EXPERIMENTAL SETUP

To evaluate the proposed blind mean SAM and ERGAS estimation framework, we constructed a dataset derived from two hyperspectral sources: the HyperSkin [14] and In-Vivo Brain [15] biomedical HSI datasets. Each hyperspectral cube was divided into non-overlapping 256×256 patches. For each patch, a synthetic low-resolution version was generated using the standard bicubic downsampling protocol commonly adopted in HSI-SR benchmarking, and super-resolved using three representative SR architectures (SSPSR [16], EUNet [17], and MambaHSISR [18]) at scale factors $\times 2$ and $\times 4$. This process resulted in 3,400 super-resolved samples: 950 at $\times 2$ and 950 at $\times 4$ for HyperSkin, and 750 at $\times 2$ and 750 at $\times 4$ for In-Vivo Brain. For each reconstructed cube, the corresponding mean SAM and ERGAS values were computed with respect to the ground truth and used as supervision, yielding paired training data $\{X_{\mathrm{SR}}, \mathrm{SAM}, \mathrm{ERGAS}\}$. Each dataset and scale factor formed a separate experiment, with its own estimator trained on a random 70% of the samples and tested on the remaining 30%.

After training, the proposed estimator trained at the matching scale is applied to generate blind quality measurements for real super-resolved hyperspectral images. In this stage, full-resolution SR outputs are produced from the original datasets at $\times 2$ (512×512) and $\times 4$ (1024×1024) scales. Since no ground-truth cubes exist at these resolutions, the trained network instead estimates mean SAM and ERGAS directly from the reconstructed cube, without reference-based computation. Prediction accuracy is assessed using Mean Squared Error (MSE), Mean Absolute Error (MAE), and Root Mean Squared Error (RMSE), together with the Pearson Linear Correlation Coefficient (PLCC), Spearman Rank-Order Correlation Coefficient (SROCC), and Kendall Rank Correlation Coefficient (KRCC).

5. RESULTS AND DISCUSSION

The results in Table 1 show that FEGAN agrees strongly with reference-computed SAM and ERGAS on both datasets. For SAM, it gives the lowest MAE and RMSE and the highest PLCC, SROCC, and KRCC. FSSAN and SFRN show higher errors but retain high correlation. For ERGAS, FEGAN holds the highest correlation on both datasets and the lowest error on In-Vivo Brain, falling slightly behind SFRN on HyperSkin.

Figure 1 confirms that the FEGAN-based estimator preserves relative performance trends and scale-dependent distortion behavior across SR methods and performs consistently across the three SR architectures and both scales, consistent with Table 1. While the predictors correlate strongly within the supported resolution regime, extrapolation beyond native hardware resolution is inherently ill-posed; occasional outliers in the in-vivo data reflect domain shift rather than systematic failure. Since FEGAN was the most consistent model, it was used to evaluate the true super-resolved images. Table 2 compares ground-truth distortion under synthetic degradation (Ref. SAM, Ref. ERGAS) with FEGAN's blind estimates on real SR outputs (Est. SAM, Est. ERGAS). The estimates correctly identify SSPSR as the method with the lowest SAM in every case. The relative ordering of EUnet and MambaHSISR is not preserved in any of the four dataset and scale settings, and since no reference exists at these scales, Table 2 supports

Table 1. Unified performance comparison for SAM and ERGAS prediction across two hyperspectral datasets. Best values are highlighted in bold.

Dataset	Model	SAM						ERGAS					
		MSE	MAE	RMSE	PLCC	SROCC	KRCC	MSE	MAE	RMSE	PLCC	SROCC	KRCC
HyperSkin	**FEGAN**	8.07×10^{-5}	**0.0069**	**0.0090**	**0.9952**	**0.9794**	**0.8840**	1.9469	1.1208	1.3953	**0.9920**	**0.8411**	**0.6836**
	FSSAN	2.42×10^{-4}	0.0126	0.0156	0.9796	0.8952	0.7332	2.0301	1.1553	1.4248	0.9896	0.7539	0.5954
	SFRN	1.50×10^{-4}	0.0099	0.0122	0.9873	0.9174	0.7763	**1.7697**	**1.0562**	**1.3303**	0.9916	0.7911	0.6368
In-Vivo Brain	**FEGAN**	2.34×10^{-4}	**0.0109**	**0.0153**	**0.9950**	**0.9874**	**0.9129**	**2.4838**	**1.2227**	**1.5760**	**0.9942**	**0.9399**	**0.8053**
	FSSAN	3.39×10^{-4}	0.0143	0.0184	0.9937	0.9842	0.8973	24.4356	3.5678	4.9432	0.9284	0.8315	0.6396
	SFRN	5.89×10^{-4}	0.0177	0.0243	0.9890	0.9816	0.8872	18.4210	3.1893	4.2920	0.9492	0.8727	0.6773

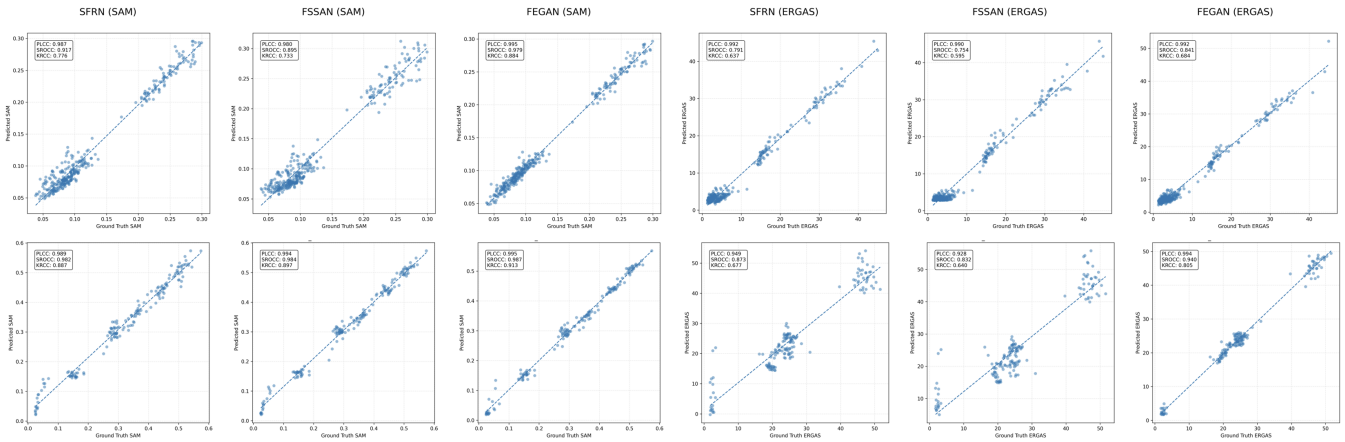


Fig. 1. Comparison of SAM and ERGAS metrics for models SFRN, FSSAN, and FEGAN. The first row shows the results for the HyperSkin dataset, and the second row corresponds to the In-Vivo Brain dataset.

Table 2. Quantitative comparison between Reference based SAM and ERGAS values (Ref. SAM, Ref. ERGAS), averaged over test patches, versus blind estimates (Est. SAM, Est. ERGAS) using FEGAN for true super resolved images on the HyperSkin and In-Vivo Brain datasets.

Method	Scale	HyperSkin				In-Vivo Brain			
		Est. SAM↓	Est. ERGAS↓	Ref. SAM↓	Ref. ERGAS↓	Est. SAM↓	Est. ERGAS↓	Ref. SAM↓	Ref. ERGAS↓
SSPSR [16]	×2	0.0817	4.41	0.071	3.52	0.101	6.14	0.134	10.01
	×4	0.228	20.03	0.090	5.09	0.229	10.37	0.1853	14.21
EUnet [17]	×2	0.092	4.61	0.103	5.81	0.321	20.61	0.4637	30.516
	×4	0.235	19.48	0.109	6.94	0.363	21.29	0.475	35.15
MambaHSISR [18]	×2	0.233	27.86	0.099	5.43	0.356	41.15	0.357	28.65
	×4	0.289	33.81	0.108	6.81	0.398	21.29	0.378	27.65

agreement in trends rather than exact values. On HyperSkin at $\times 2$ the estimates stay close to ground truth for SSPSR, with larger gaps for EUnet and MambaHSISR, especially ERGAS at $\times 4$, reflecting stronger spatial variability and the greater difficulty of predicting ERGAS from the reconstructed signal alone. On In-Vivo Brain the estimator tracks both trends more closely. Overall, the proposed FEGAN predictor largely preserves the scale-dependent behavior of the SR methods, supporting its use as a practical blind quality indicator.

6. CONCLUSION

This letter introduced a blind distortion estimation framework that predicts proxy estimates of SAM and ERGAS directly from super-resolved hyperspectral cubes without access to ground-truth. The approach relies on spectral–spatial representations that capture angular and spatial–spectral distortion patterns, and it was trained using distortion values computed under the standard synthetic evaluation protocol. Experiments on biomedical HSI datasets show that the estimator closely follows the trends observed in reference-based evalu-

ation and performs consistently across the three SR architectures and both scales. This provides a simple and effective tool for evaluating HSI super-resolution models when high-resolution references are unavailable. As the estimates are learned proxies, future work includes testing across datasets and on unseen SR methods.

7. REFERENCES

[1] W.-j. Guo, W. Xie, K. Jiang, Y. Li, J. Lei, and L. Fang, "Toward Stable, Interpretable, and Lightweight Hyperspectral Super-Resolution," in *2023 IEEE/CVF Conference on Computer Vision and Pattern Recognition (CVPR)*, pp. 22272–22281, 2023.

[2] Z. Dehghan, J. Yang, A. Khader, J. Fang, and L. Xiao, "Learning Spectral–Spatial-Former Deep Prior for Hyperspectral Image Superresolution," *IEEE Journal of Selected Topics in Applied Earth Observations and Remote Sensing*, vol. 18, pp. 17926–17943, 2025.

[3] S. Jiang, N. Li, M. Xu, S. Zhang, and S. Jia, "SQ-former: Spectral-Query Transformer for Hyperspectral Image Arbitrary-Scale Super-Resolution," *IEEE Transactions on Geoscience and Remote Sensing*, vol. 62, pp. 1–15, 2024.

[4] C. Chen *et al.*, "A review of hyperspectral image super-resolution based on deep learning," *Remote Sensing*, vol. 15, no. 11, p. 2853, 2023.

[5] N. Zhang and W. H. Mahmoud, "Target Detection in Hyperspectral Imagery Using Spectral Signature Matching Algorithms," in *2025 13th International Conference on Intelligent Control and Information Processing (ICICIP)*, pp. 108–114, 2025.

[6] J. Yang, Y.-Q. Zhao, C. Yi, and J. C.-W. Chan, "No-reference hyperspectral image quality assessment via quality-sensitive features learning," *Remote Sensing*, vol. 9, no. 4, p. 305, 2017.

[7] X. Meng, K. Bao, J. Shu, B. Zhou, F. Shao, W. Sun, and S. Li, "A Blind Full-Resolution Quality Evaluation Method for Pansharpening," *IEEE Transactions on Geoscience and Remote Sensing*, vol. 60, pp. 1–16, 2022.

[8] X. Hao, X. Li, J. Wu, B. Wei, and L. Li, "A Review of No-Reference Quality Assessment for Hyperspectral Sharpening," in *2023 11th International Conference on Information Systems and Computing Technology (ISCTech)*, pp. 74–80, 2023.

[9] Y. Li, Y. Dong, H. Li, D. Liu, F. Xue, and D. Gao, "No-reference hyperspectral image quality assessment via ranking feature learning," *Remote Sensing*, vol. 16, no. 10, p. 1657, 2024.

[10] Z. Zhang, W. Sun, X. Min, W. Zhu, T. Wang, W. Lu, and G. Zhai, "A no-reference deep learning quality assessment method for super-resolution images based on frequency maps," in *2022 IEEE International Symposium on Circuits and Systems (ISCAS)*, pp. 3170–3174, 2022.

[11] R. Dian, L. Fang, and S. Li, "Hyperspectral Image Super-Resolution via Non-local Sparse Tensor Factorization," in *2017 IEEE Conference on Computer Vision and Pattern Recognition (CVPR)*, pp. 3862–3871, 2017.

[12] T. Zhang, Y. Fu, and C. Li, "Hyperspectral Image Denoising with Realistic Data," in *2021 IEEE/CVF International Conference on Computer Vision (ICCV)*, pp. 2228–2237, 2021.

[13] P. Zhang, D. Zhao, Y. Ma, and W. Chu, "Hyperspectral Image Super-Resolution via Wavelet Decomposition Guidance and Cross-Dimensional Feature Interaction," *IEEE Journal of Selected Topics in Applied Earth Observations and Remote Sensing*, vol. 18, pp. 28422–28438, 2025.

[14] P. C. Ng, Z. Chi, Y. Verdie, J. Lu, and K. N. Plataniotis, "Hyper-skin: A hyperspectral dataset for reconstructing facial skin-spectra from rgb images," in *Advances in Neural Information Processing Systems* (A. Oh, T. Naumann, A. Globerson, K. Saenko, M. Hardt, and S. Levine, eds.), vol. 36, pp. 24158–24170, Curran Associates, Inc., 2023.

[15] H. Fabelo, S. Ortega, A. Szolna, D. Bulters, J. F. Piñeiro, S. Kabwama, A. J-O'Shanahan, H. Bulstrode, S. Bisshopp, B. R. Kiran, D. Ravi, R. Lazcano, D. Madroñal, C. Sosa, C. Espino, M. Marquez, M. De La Luz Plaza, R. Camacho, D. Carrera, M. Hernández, G. M. Callicó, J. Morera Molina, B. Stanciulescu, G.-Z. Yang, R. Salvador, E. Juárez, C. Sanz, and R. Sarmiento, "In-vivo hyperspectral human brain image database for brain cancer detection," *IEEE Access*, vol. 7, pp. 39098–39116, 2019.

[16] J. Jiang, H. Sun, X. Liu, and J. Ma, "Learning spatial-spectral prior for super-resolution of hyperspectral imagery," *IEEE Transactions on Computational Imaging*, vol. 6, pp. 1082–1096, 2020.

[17] D. Liu, J. Li, Q. Yuan, L. Zheng, J. He, S. Zhao, and Y. Xiao, "An efficient unfolding network with disentangled spatial-spectral representation for hyperspectral image super-resolution," *Information Fusion*, vol. 94, pp. 92–111, 2023.

[18] Y. Xu, H. Wang, F. Zhou, C. Luo, X. Sun, S. Rahardja, and P. Ren, "Mambahsisr: Mamba hyperspectral image super-resolution," *IEEE Transactions on Geoscience and Remote Sensing*, vol. 63, pp. 1–16, 2025.